

Article

# DOA Estimation for Underwater Target by Active Detection on Virtual Time Reversal Using a Uniform Linear Array

Haixia Jing <sup>1,2</sup>, Haiyan Wang <sup>1,\*</sup>, Zhengguo Liu <sup>3</sup> and Xiaohong Shen <sup>1</sup>

<sup>1</sup> School of Marine Science and Technology, Northwestern Polytechnical University, Xi'an 710072, China; haixjing@gmail.com (H.J.); xhshen@nwpu.edu.cn (X.S.)

<sup>2</sup> School of Engineering, Xi'an International University, Xi'an 710077, China

<sup>3</sup> China Shipbuilding Industry Corporation, Beijing 100097, China; liuzg@csic.com.cn

\* Correspondence: hywang@nwpu.edu.cn; Tel.: +86-29-88-495-759

Received: 16 June 2018; Accepted: 25 July 2018; Published: 29 July 2018



**Abstract:** Aiming at addressing the problem caused by multipath effects in direction of arrival (DOA) estimation for underwater targets, a method based on the active detection on virtual time reversal (ADVTR) Capon algorithm is proposed. Unlike the conventional passive target estimation method ignoring the multipath effects but only considering the direct wave, the proposed method is closer to the actual situation in that the multipath signal propagation model is fully taken into account; in addition, active detection (AD) and virtual time reversal (VTR) processes are added, which use active detection to estimate channels, and virtual time reversal to realize focusing in a computer after the source-receive array (SRA) receives the reflected signal of the target. The combination of the two methods can greatly improve the energy of SRA and the precision of target direction estimation. With the popular acoustic field simulation tool Bellhop, the model proposed in this paper is verified. Compared with the conventional Capon method without time reversal, the simulation results show that the ADVTR Capon estimation method is far better, in terms of resolution and suppressing the sidelobes. It is suitable for the target DOA estimation under low signal-to-noise ratio (SNR) conditions. Further, we also show the ADVTR Capon estimation method works well in a real tank experiment.

**Keywords:** active detection on virtual time reversal (ADVTR); direction of arrival (DOA) estimation; multipath effects; ULA; Capon algorithm; spatial smoothing

## 1. Introduction

Direction of arrival (DOA) estimation is an important part of the target parameter estimation which has found broad applications in radar, sonar, wireless communication and so on [1]. There have been a large number of DOA estimation algorithms in the past few decades, including Conventional Beamforming, Capon Minimum Variance Method (MVM), Multiple Signal Classification (MUSIC, Estimation of Signal Parameters via Rotational Invariance Techniques (ESPRIT, Maximum Likelihood (ML) estimation, Weighted Subspace Fitting (WSF) algorithm, etc. [2]. Compressed Sensing (CS) [3,4] DOA estimation technology proposed in recent years also shows good performance with little less snapshots [5,6]. In addition, there are various DOA estimation methods for different applications and environments, such as those described in [2,7,8].

The aforementioned methods are usually based on the traditional direct-path-only assumption, where multipath is ignored or considered detrimental and a negative whose effect impacts the performance of the algorithm especially at low signal-to-noise ratio (SNR) so as to be minimized or eliminated [9,10]. The technique of time reversal (TR), on the contrary, treats multipath a positive,

which can self-adaptively modify the signal distortion caused by multipath effect and make the target get spatial-temporal focusing at source location [11], the more the better [12]. For the concrete theory and methods on TR readers can refer to the reviews of [13–15]. The self-focusing nature of TR has subsequently been verified in ultrasonic [16], acoustic [17], underwater acoustic [18–20] and electromagnetic fields [21,22] and achieved extensive applications in imaging [23], detection [24–26], localization [27,28], communication [29–31], DOA estimation [32] and other domains [33]. In this paper, we will focus on the DOA estimation by TR on multipath and low SNR conditions, and attempt to establish the TR multipath DOA model for underwater acoustics from the array signal processing perspective.

Asif's research team has published many articles on this subject by active time reversal (ATR) in radar domain [32,34–39]. In [32] and [34], a TR DOA estimator for a passive target in a Ground Penetrating Radar (GPR) and a mobile communication network are studied, respectively. The performance of the DOA estimator with and without TR is compared and the simulation results show that the performance of the DOA estimator with TR is superior to the conventional approach. Furthermore, TR/range estimator is added and the active array source location for a single target is accomplished [35]. In [36], a TR-based DOA estimation framework for multiple-input multiple-output (MIMO) radars is presented. Reference [37] introduces TR into the Angle-Doppler estimation in MIMO radars and the closed-form expressions of Cramér-Rao bound (CRB) for DOA and Doppler frequency of a moving target in MIMO and TR/MIMO are derived in [38]. Reference [39] applies the compressive sensing (CS) and TR to MIMO radars to achieve the joint estimation of DOA, direction of departure (DOD) and Doppler information. In addition, Fu [40] proposes a virtual time reversal (VTR) method for the DOA estimation of electromagnetic signal emitted from a single communication station passively, which can determine the azimuth of the radiation source by finding the maximum energy points in the scanning area. Ciunozzo et al. [41–43] studies the performance of multiple signal classification (MUSIC) for computational time reversal (computational TR is VTR [44,45]) applications. Reference [46] addresses a DOA estimation method by passive time reversal (PTR) in a low angle target parameter estimation and antenna array scenario. Song referred to VTR proposed in [47] as PTR in the overview of underwater TR communication [31] and we will follow this statement in the later discussion. More information on ATR, PTR and VTR will be discussed in Section 2. The above TR DOA estimation method in the electromagnetic field is useful for DOA estimation of underwater target by TR.

In the underwater scenario, Reference [48] utilizes PTR to study the DOA estimation performance of a uniform shallow sea target, which proposes a super-directional model based on non-uniform linear array (NLA), establishes the simulation model from the signal detection point of view and uses the conventional beamforming method to achieve the azimuth estimation at low SNR. A PTR target orientation algorithm under Doppler spread is proposed for underwater acoustic multipath time-varying channel in [49] and the target orientation can be realized accurately by frequency compensation and time reversal processing.

From the above discussions, we can see that the current TR DOA estimation methods mainly focus on the ATR and VTR, which have the following problems. First, the methods based on ATR needs two signal transmissions so that the attenuation of energy is greater and receiving SNR of the array is reduced, thus affecting the estimation performance, especially for the weak target. Then although there is only one receiving process in PTR, it needs to first solve the problem how to obtain the real channel exactly in that only when the analog channel and actual one are completely matched can the ideal TR spatial-temporal focusing effect and accurate DOA estimation be achieved. To solve the above problems, an improved method called virtual TR based on active detection (ADVTR) is proposed in [50] to accomplish uniform linear array (ULA) beamforming, which establishes the required model from the perspective of signal detection, and estimates the angle by conventional beamforming method. Combining the advantages of ATR with PTR, the first process of ADVTR will realize the detection and channel estimation in the real channel and the second process will complete TR focusing virtually in

the computer. Compared with ATR, there is no real re-emitting process so that the second receiving process has no noise in ADVTR and the SNR of the array received signal are higher; Compared with PTR, the characteristics of ocean channels can be estimated ideally according to the active detection while avoiding the PTR approximation process on the basis of the same processing gain with PTR.

There are few references on the ADVTR method: in addition to [50], the method is also intended for target detection in [51]. Based on [50,51], we propose in this paper a DOA estimation method based on ADVTR for underwater multiple targets from array signal processing perspective. It can exploit the underwater multipath propagation channel to improve the SNR of the received signal and the accuracy of target DOA estimation, especially at low SNR. We believe the method proposed in this paper can be applied in underwater search & rescue, wreck salvage and other fields as well. The main contribution in this context is as follows:

- (1) An ADVTR Capon method is proposed to improve the performance of DOA estimation at low SNR;
- (2) The model of conventional multipath and ADVTR multipath for ULA are established based on underwater acoustics propagation theory and array signal processing theory;
- (3) In contrast with the method in [50] which is only confirmed through simulation, the performance of ADVTR Capon algorithm is verified and analyzed by simulation and tank experiment;
- (4) Our model and method in this paper are readily extended to the DOA estimation of two or more targets with respect to [50], while [50] can only achieve one target's orientation.

The rest of this paper is organized as follows: the ADVTR method is introduced in Section 2. A system model based on multipath is deduced in details in Section 3. Section 4 reviews the spatial smoothing and conventional Capon algorithm firstly, and then presents the ADVTR Capon algorithm based on spatial smoothing. The performance of the proposed ADVTR Capon algorithm is analyzed using the simulated data from Bellhop acoustic field simulation in Section 5. Section 6 illustrates the anechoic tank experiment and the DOA estimation results. Conclusions and future works are given in Section 7.

Notation: Lower and upper case boldface letters denote vectors and matrices, respectively;  $(\cdot)^*$ ,  $(\cdot)^T$ ,  $(\cdot)^H$  and  $(\cdot)^{-1}$  stand for conjugate, transpose, Hermitian transpose and inverse, respectively;  $E\{\cdot\}$  is the expected value of a random quantity;  $\otimes$  is the convolution of two signal and  $\odot$  is the Hadamard product of two vectors or matrices, i.e., the vector or matrix of their components wise product.

## 2. The Principle of ADVTR

In this section, we mainly discuss the principle of ADVTR method and then give the flow diagram of the DOA estimation method based on ADVTR.

TR, known as phase conjugation (PC) in optics, is a process of transmitting the received signal on an array in a time-reversed order, and then due to spatial reciprocity and TR invariance of the linear acoustic wave equation, the retransmitted signal converges back to the position where the original signal was generated [31]. If the retransmitted signal is actually transmitted over the real medium, it is referred to as a so-called physical TR, while if the back-propagation is computed or done numerically, in a fictitious, reference medium, it is called computational or virtual TR [43,44]. Dowling [52] first proposed the concept of ATR and PTR and pointed out that PTR processing is related to ATR by invoking reciprocity for a measured acoustic signal as a replacement for the back-propagation step of ATR. Therefore, according to whether the process of back-propagation is performed in the real medium, PTR is also regarded as VTR.

ATR, PTR and ADVTR have been used for target detection in [51,53,54]. Here we will refer to above publications to compare the difference between ATR, PTR and ADVTR. The diagrams of ATR, PTR and ADVTR are shown in Figure 1.

For ATR [53], as shown in Figure 1a, the process can be divided into two phases. During phase 1, the transducer emits a detection signal  $s(t)$  through the underwater acoustic channel  $h_1(t)$  to illuminate possible targets and receives reflected signal  $y(t)$  through the channel  $h_2(t)$ . During phase 2, the time reversed signal  $y(-t)$  is re-transmitted to the same channel as phase 1 once again. The transducer receives the signal  $z(t)$  during phase 2.

For PTR [54], as shown in Figure 1b, the radiation signal from the target  $s(t)$  is received by the hydrophone through channel I,  $y(t)$  corresponds to the reception signal with the additive noise  $n(t)$ , which is different with ATR in that it doesn't send signal again and channel II is simulated by computer. Only when channel I and channel II match with each other, the energy focus can be achieved.

For ADVTR [51], as shown in Figure 1c, the dashed line of ATR in Figure 1a or phase 2 of ATR is done virtually in a computer. To illustrate the "active detection (AD)" and "virtual TR (VTR)" of the method more clearly, the diagram is expressed as shown in Figure 1c, which is separated into two parts by the dash line. Firstly, in the active part, the transducer emits a detection signal  $s(t)$  through underwater acoustic channel  $H_1(t)$  to the interested area and receives the reflected signal  $y(t)$  from a target. Then the virtual underwater acoustic channel  $H_2(t)$  can be estimated by comparing the emitted signal  $s(t)$  with the received signal  $y(t)$  in the virtual part. Finally, the time reversed signal  $y(-t)$  is transmitted virtually through the virtual channel  $H_2(t)$  and detected by the detector. Note,  $H_1(t)$  in (c) is equal to  $h_1(t) \otimes h_2(t)$  in (a).

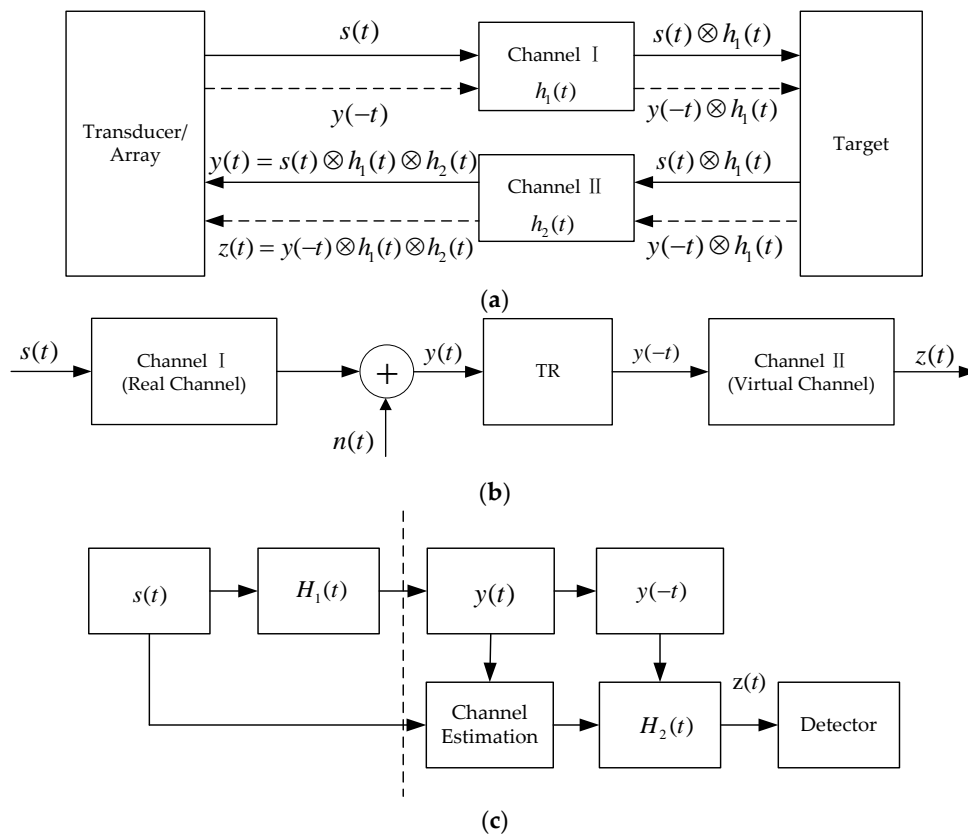


Figure 1. Diagram of ATR, PTR and ADVTR. (a) ATR; (b) PTR; (c) ADVTR.

The principles on ATR and PTR can refer to [53,54]. Here we only discuss the ADVTR. The received signal  $y(t)$  can be expressed as:

$$y(t) = s(t) \otimes H_1(t) + n(t) \tag{1}$$

where  $n(t)$  denotes environment noise.

Virtual time reversal is carried out for (1), and then the signal  $z(t)$  can be expressed as:

$$z(t) = s(-t) \otimes H_1(-t) \otimes H_2(t) + n(-t) \otimes H_2(t) \quad (2)$$

If the virtual channel  $H_2(t)$  could match the true channel  $H_1(t)$ , i.e.,  $H_1(t) = H_2(t) = H(t)$ , Equation (2) can be rewritten as:

$$z(t) = s(-t) \otimes \int_{-\infty}^{+\infty} h^2(t)dt + n(-t) \otimes h_2(t) \quad (3)$$

From Equation (3), we can observe that time reversal could utilize the multi-path effect to strengthen the detected signal, and consequently improve the detection performance. The other observation from Equation (3) is that the output of ADVTR process has the same expression as PTR. Obviously, ADVTR reduces the number of transmissions to one, and has more focusing ability compared with ATR.

Furthermore, combined with DOA estimation, we can obtain the flow diagram of the DOA estimation based on ADVTR as shown in Figure 2. First, PS transmits a detection signal to illuminate possible targets actively; then the sensors receive reflected signal and the environment noise should be considered. Several operations will be performed in the computer virtually, including filtering, channel estimating, VTR, re-emitting, receiving secondly and DOA estimation. Because of the AD, the frequency of received signal has been known, then filtering is performed before VTR and the virtual underwater acoustic channel can be estimated by comparing the emitted signal with the received signal. The TR signal of each sensor is re-emitted to the estimated channel virtually in the computer and the sensors receive the reflected signal once again and DOA estimation is done finally.

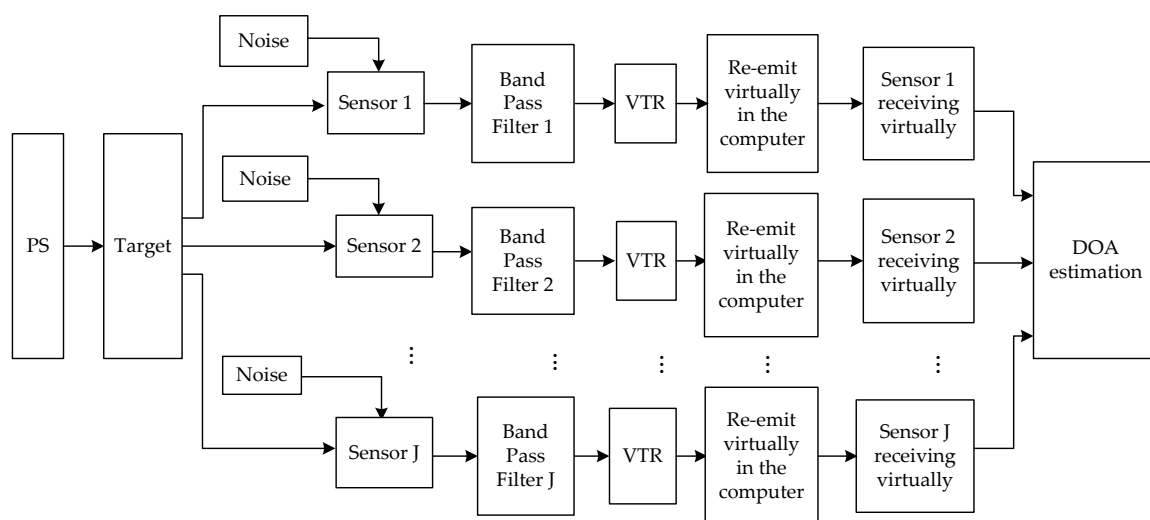


Figure 2. Flow diagram of the DOA estimation based on ADVTR.

### 3. Multipath DOA Estimation Model for ULA Based on ADVTR

Based on underwater acoustics propagation theory and array signal processing theory, we derive the conventional multipath and ADVTR multipath DOA model for ULA respectively in this section.

#### 3.1. Multipath Model Diagram for ULA

The multipath DOA estimation model diagram for ULA based on the ray theory is shown in Figure 3. SRA in Figure 3 is the vertical ULA, whose element number is  $J$  and interelement spacing is  $d$ . For convenience, only three propagation paths between the target and SRA are drawn: the direct-path, the top-reflection-path and the bottom-reflection-path, whose incident angle (i.e., DOA of backscatter

from target propagating via various paths) are as follows:  $\theta_1, \theta_2$  and  $\theta_3$ . To be more general, the acoustic propagation paths deduced subsequently are not confined to these three paths, but  $N$  or  $M$ .

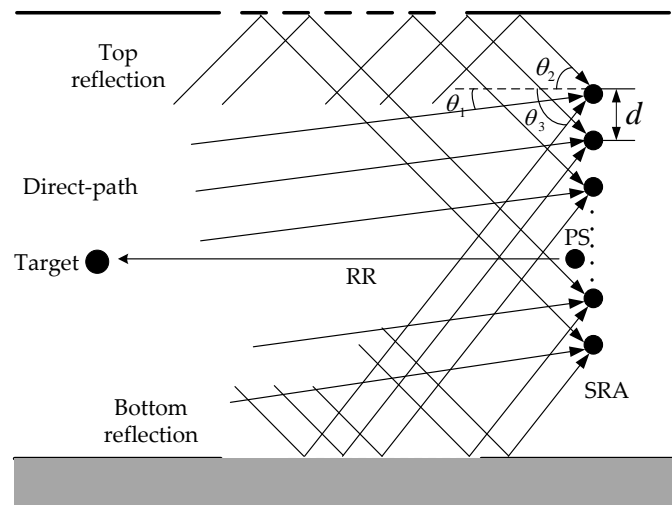


Figure 3. Multipath DOA estimation diagram for ULA.

### 3.2. Conventional Multipath DOA Model for ULA

Firstly, PS located in element  $k$  of SRA will transmit the signal  $f(t)$ . According to ray theory, the channel transfer function between the transmitting acoustic source and the target can be expressed as:

$$h_k(t) = \sum_{n=1}^N c_{kn} \delta(t - \tau_{kn}) \quad (4)$$

where  $N$  is the total number of sound ray;  $c_{kn}$  is the amplitudes (or attenuation) of  $n$ -th eigen ray (also regarded as the propagation path) from element  $k$  to target; and  $\tau_{kn}$  is the travel times (or delay) of  $n$ -th eigen ray from element  $k$  to target. On the basis of (4), the signal received by the target can be expressed as (5):

$$x_k(t) = f(t) \otimes h_k(t) = \sum_{n=1}^N c_{kn} f(t - \tau_{kn}) \quad (5)$$

Assuming that the target reflection coefficient is 1, and considering the effect of noise from reception process, the signal received by the element  $j$  is:

$$\begin{aligned} y_j(t) &= x_k(t) \otimes h_j(t) + v_j(t) \\ &= \sum_{n=1}^N c_{kn} f(t - \tau_{kn}) \otimes \sum_{m=1}^M c_{jm} \delta(t - \tau_{jm}) + v_j(t) \\ &= \sum_{m=1}^M \sum_{n=1}^N c_{jm} c_{kn} f(t - \tau_{jm} - \tau_{kn}) + v_j(t) \end{aligned} \quad (6)$$

where  $h_j(t)$  represents the channel function between the target and element  $j$ ;  $v_j(t)$  is the environment noise received by element  $j$ .  $c_{jm}$  and  $\tau_{jm}$  represent amplitudes and travel times of the  $m$ -th propagation path from target to element  $j$  separately.

Suppose the transmitter signal as  $f(t) = s(t)e^{j\omega_c t}$ . Combining far field and narrow band model theory of array signal processing [1], Equation (6) can be expressed as:

$$\begin{aligned}
 y_j(t) &= \sum_{m=1}^M \sum_{n=1}^N c_{jm} c_{kn} f(t - \tau_{kn} - \tau_{1m} - \Delta\tau_{jm}) + v_j(t) \\
 &\approx \sum_{m=1}^M \sum_{n=1}^N c_{jm} c_{kn} s(t) e^{j\omega_c(t - \tau_{kn} - \tau_{1m} - \Delta\tau_{jm})} + v_j(t) \\
 &= \sum_{m=1}^M c_{jm} e^{-j\omega_c \Delta\tau_{jm}} e^{-j\omega_c \tau_{1m}} \cdot \sum_{n=1}^N c_{kn} e^{-j\omega_c \tau_{kn}} \cdot s(t) e^{j\omega_c t} + v_j(t)
 \end{aligned} \tag{7}$$

where  $\tau_{1m}$  represents the reference delay associated with backscatter from target traveling via path  $m$  to element 1 (the reference element); and  $\Delta\tau_{1m}$  is the interelement delay associated with path  $m$  originating from target in excess of  $\tau_{1m}$  with respect to the receiving element  $j$ .

The received signals of element  $j$  expressed in (7) is generalized to other array elements and expressed in the matrix form as:

$$\mathbf{Y}(t) = (\mathbf{C} \odot \mathbf{A}) \mathbf{D} \mathbf{X}_k \mathbf{F}(t) + \mathbf{V}(t) \tag{8}$$

where the symbol “ $\odot$ ” is the Hadamard Product or Basic Product, which can realize the point-to-point product of two identical-order matrices;  $\mathbf{Y}(t) = [y_1(t), \dots, y_J(t)]^T$  is defined as the received signal matrix received by the element 1 –  $J$  of the SRA;  $\mathbf{C}$  is a  $(J \times M)$  matrix representing the attenuation matrix with respect to the channel response function between the target and SRA elements, whose element  $c_{jm}$  indicates the attenuation associated with backscatter from target traveling via path  $m$  to element  $j$ ;  $\mathbf{A}$  is a  $(J \times M)$  matrix representing a relative delay matrix to the reference element (element 1) and given by (9);  $\mathbf{D} = [e^{-j\omega_c \tau_{11}}, e^{-j\omega_c \tau_{12}}, \dots, e^{-j\omega_c \tau_{1M}}]^T$  is the reference delay matrix including interrelated delay from target traveling via all  $M$  paths to element 1;  $\mathbf{X}_k$  expressed as Equation (10) can be considered as a target-received signal matrix which is transmitted from the element  $j$  through the channel to the target;  $\mathbf{F}(t) = s(t) e^{j\omega_c t}$  is called the transmitting matrix; and  $\mathbf{V}(t)$  indicates the noise matrix:

$$\mathbf{A} = \begin{bmatrix} e^{-j\omega_c \Delta\tau_{11}} & e^{-j\omega_c \Delta\tau_{12}} & \dots & e^{-j\omega_c \Delta\tau_{1M}} \\ e^{-j\omega_c \Delta\tau_{21}} & e^{-j\omega_c \Delta\tau_{22}} & \dots & e^{-j\omega_c \Delta\tau_{2M}} \\ \vdots & \vdots & \vdots & \vdots \\ e^{-j\omega_c \Delta\tau_{J1}} & e^{-j\omega_c \Delta\tau_{J2}} & \dots & e^{-j\omega_c \Delta\tau_{JM}} \end{bmatrix} \tag{9}$$

$$\mathbf{X}_k = \sum_{n=1}^N c_{kn} e^{-j\omega_c \tau_{kn}} = (\mathbf{C}(k, :)) \odot \mathbf{A}(k, :)) \mathbf{D} \tag{10}$$

Referring to array signal processing theory [1], when the array interelement spacing of ULA is  $d$ , Equation (9) can be represented as (11):

$$\begin{aligned}
 \mathbf{A} &= [\mathbf{a}(\theta_1), \mathbf{a}(\theta_2), \dots, \mathbf{a}(\theta_M)] \\
 &= \begin{bmatrix} 1 & 1 & \dots & 1 \\ e^{-j\frac{2\pi}{\lambda} d \sin \theta_1} & e^{-j\frac{2\pi}{\lambda} d \sin \theta_2} & \dots & e^{-j\frac{2\pi}{\lambda} d \sin \theta_M} \\ \vdots & \vdots & \vdots & \vdots \\ e^{-j\frac{2\pi}{\lambda} (J-1) d \sin \theta_1} & e^{-j\frac{2\pi}{\lambda} (J-1) d \sin \theta_2} & \dots & e^{-j\frac{2\pi}{\lambda} (J-1) d \sin \theta_M} \end{bmatrix}
 \end{aligned} \tag{11}$$

$\mathbf{A}$  of Equation (9) is known as the array steering matrix (DOA matrix) that contains all multipath information, and mainly depends on the array structure and the direction of arrival, where  $m$ -th column  $\mathbf{a}(\theta_m)$  is known as steering vector and denotes the received information from target via path  $m$  to each element;  $\theta_m$  is the angle information of path  $m$  from target to each element.

As mentioned, the method proposed in the paper is to add some additional stages such as TR, re-emitting, reflecting by target and receiving of SRA on the basis of conventional DOA estimation. Therefore the following discussion will devote to the establishment of a multipath DOA model based on ADVTR.

### 3.3. ADVTR Multipath DOA Model for ULA

According to the flow of ADVTR mentioned in Section 2, the first process of ADVTR is active detection, so the frequency of the transmitted signal has been known when the array receives the signal. Then the filter can be introduced to eliminate the impact of noise before TR operation. Subsequently VTR is performed virtually for the received signals of each SRA in the computer, and taking element  $j$  as an example:

$$y_j(-t) = B \cdot s(-t)e^{-j\omega_c t} = Bf(-t) \quad (12)$$

where  $B$  is expressed as (13), whose value is independent of time  $t$  and can be considered as a coefficient:

$$B = \left( \sum_{m=1}^M c_{jm} e^{-j\omega_c \Delta\tau_{jm}} e^{-j\omega_c \tau_{1m}} \right) \cdot \sum_{n=1}^N c_{kn} e^{-j\omega_c \tau_{kn}} \quad (13)$$

The signal expressed as (12) is energy normalized and then re-transmitted virtually into the channel as a secondary transmission signal in the computer, which still satisfies the far field and narrow band model theory. Repeat the above first procedure, refer to Equations (4)–(7), and suppose the signal received by element  $l$  is  $z_l(t)$ :

$$\begin{aligned} z_l(t) &\approx \sum_{m=1}^M \sum_{n=1}^N c_{lm} c_{jn} g_j B s(-t) e^{-j\omega_c (t - \tau_{jm} - \tau_{1m} - \Delta\tau_{lm})} \\ &= \sum_{m=1}^M c_{lm} e^{j\omega_c \Delta\tau_{lm}} e^{j\omega_c \tau_{1m}} \cdot \sum_{n=1}^N c_{jn} e^{j\omega_c \tau_{jn}} \cdot g_j B s(-t) e^{-j\omega_c t} \end{aligned} \quad (14)$$

where  $g_j$  is the normalized coefficient of element  $j$  obtained with reference to the transmitted signal power, and owing to the principle of virtual time reversal, the secondary process has no noise.

Referring to (8)–(11), the received signal of all of elements of SRA on the second time with element  $j$  probing virtually is:

$$\mathbf{Z}_j(t) = (\mathbf{C} \odot \mathbf{A}^*) \mathbf{D}^* \mathbf{X}_j^* g_j y_j(-t) \quad (15)$$

where  $\mathbf{A}$ ,  $\mathbf{C}$ ,  $\mathbf{D}$  are the same as the parameters of (5), and  $\mathbf{X}_j$  is the same as  $\mathbf{X}_k$  of (8) except that  $\mathbf{X}_k$  is the received signal matrix with element  $k$  probing,  $\mathbf{X}_j$  is the received signal matrix with element  $j$  probing.

The received signals with element  $j$  of SRA probing expressed as (15) are generalized to other array elements and the sum of received signals of SRA after TR is:

$$\begin{aligned} \mathbf{Z}_{tr} &= \sum_{j=1}^J \mathbf{Z}_j(t) \\ &= \sum_{j=1}^J (\mathbf{C} \odot \mathbf{A}^*) \mathbf{D}^* \mathbf{X}_j^* g_j y_j(-t) \\ &= (\mathbf{C} \odot \mathbf{A}^*) \mathbf{D}^* \sum_{j=1}^J \mathbf{X}_j^* g_j y_j(-t) \end{aligned} \quad (16)$$

## 4. DOA Estimation Algorithm

In order to express our method clearly, we briefly review the spatial smoothing and conventional Capon algorithm. Then, we give our DOA estimation algorithm in detail and the computational complexity of the proposed algorithm.

### 4.1. Spatial Smoothing Algorithm

Since the multipath model is introduced, the signals arriving to SRA from the target via each path are coherent signals. Therefore, spatial smoothing technique is applied into the coherent processing prior to the DOA estimation [55].

In combination with the above model in Section 3, suppose that the array is an equidistant linear array with  $J$  elements and element distance  $d$ . The  $J$  elements linear array is decomposed into  $q$  overlapping subarrays, and each subarray has  $ns$  array elements, as shown in Figure 4. In Figure 4, the relationship with  $J$ ,  $ns$  and  $q$  should satisfy the relationship of Equation (17):

$$q = J + 1 - ns \tag{17}$$

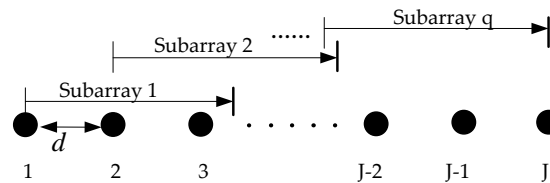


Figure 4. Spatial smoothing algorithm diagram.

The subarray  $i$  is composed of line  $i$  to line  $i + ns - 1$  of the signal matrix, and taking the array received signal  $\mathbf{Y}$  in (8) as an example, the signal matrix of subarray  $i$  can be represented as:

$$\mathbf{Y}_i(t) = [y_i(t), y_{i+1}(t), \dots, y_{i+ns-1}(t)]^T \tag{18}$$

The covariance matrix can be calculated for each subarray of (18) by:

$$\mathbf{R}_{Y_i} = E\{\mathbf{Y}_i(t)\mathbf{Y}_i(t)^H\} \tag{19}$$

Then, the spatial smoothing covariance matrix of the received signal for the first time can be obtained by averaging (19) which is expressed as (20):

$$\mathbf{R}_{YY} = \frac{1}{q} \sum_{i=1}^q \mathbf{R}_{Y_i} \tag{20}$$

Similarly, the signals received secondly shown in (16) are smoothed spatially, and the signal matrix of subarray  $i$  can be represented as:

$$\mathbf{Z}_{tri}(t) = [\mathbf{Z}_{tr}(i), \mathbf{Z}_{tr}(i + 1), \dots, \mathbf{Z}_{tr}(i + ns - 1)]^T \tag{21}$$

The covariance matrix can be calculated for each subarray of (21) by:

$$\mathbf{R}_{Z_i} = E\{\mathbf{Z}_{tri}(t)\mathbf{Z}_{tri}(t)^H\} \tag{22}$$

The spatial smoothing covariance matrix of the signal received secondly can be expressed as (23) by averaging (22):

$$\mathbf{R}_{ZZ} = \frac{1}{q} \sum_{i=1}^q \mathbf{R}_{Z_i} \tag{23}$$

#### 4.2. Conventional Multipath Capon Algorithm

According to the array signal processing theory [1], the purpose of the Capon algorithm is attempting to minimize the power by noise and other interference signal except the desired signal, while maintaining a fixed gain in the direction from which the signal originated. Combining the model established by Equation (8), the Capon algorithm can be represented as the following minimum problem:

$$\begin{aligned} &\min \mathbf{w}^H(\theta)\hat{\mathbf{R}}_Y\mathbf{w}(\theta) \\ &\text{S.T. : } \mathbf{w}^H(\theta)\mathbf{a}(\theta_1) = 1 \end{aligned} \tag{24}$$

where  $\hat{\mathbf{R}}_Y = \frac{1}{N}E\{\mathbf{Y}(t)\mathbf{Y}(t)^H\}$  is the sample covariance matrix of the array output signal with the multipath;  $\theta_1$  is desired angle information and  $\mathbf{w}$  is the weight value.

The Lagrange multiplier method can be used to obtain the solution of the above problem:

$$\mathbf{w} = \frac{\hat{\mathbf{R}}_Y^{-1}\mathbf{a}(\theta_1)}{\mathbf{a}^H(\theta_1)\hat{\mathbf{R}}_Y^{-1}\mathbf{a}(\theta_1)} \tag{25}$$

Equation (26) can be obtained by taking Equation (25) into Equation (24), which means the largest power in the desired direction while the power except the desired direction is the smallest:

$$P(\theta) = \frac{1}{\mathbf{a}^H(\theta_1)\hat{\mathbf{R}}_Y^{-1}\mathbf{a}(\theta_1)} \tag{26}$$

Thus the spatial spectrum of the Capon algorithm can be defined as:

$$P(\theta) = \frac{1}{\mathbf{a}^H(\theta)\hat{\mathbf{R}}_Y^{-1}\mathbf{a}(\theta)} \tag{27}$$

where  $\mathbf{a}(\theta)$  is the steering vector and can be defined as (28):

$$\mathbf{a}(\theta) = \left[1, e^{-j\frac{2\pi}{\lambda}d \sin \theta}, \dots, e^{-j\frac{2\pi}{\lambda}(J-1)d \sin \theta}\right]^T \tag{28}$$

### 4.3. ADVTR Capon Algorithm

According to Equation (16), follow the same steps as the above conventional DOA estimation:

$$\begin{aligned} &\min \mathbf{w}_{tr}^H(\theta)\hat{\mathbf{R}}_{Z_{tr}}\mathbf{w}_{tr}(\theta) \\ &\text{subject to : } \mathbf{w}_{tr}^H(\theta)\mathbf{a}_{tr}(\theta_1) = 1 \end{aligned} \tag{29}$$

Equation (29) is similar to (24) but  $\hat{\mathbf{R}}_{Z_{tr}} = \frac{1}{N}E\{\mathbf{Z}_{tr}(t)\mathbf{Z}_{tr}(t)^H\}$  is the sample covariance matrix after virtual time reversal output signal and the other values are the same as above. At this time, the spatial spectrum of the ADVTR Capon algorithm is:

$$P_{tr}(\theta) = \frac{1}{\mathbf{a}_{tr}^H(\theta)\hat{\mathbf{R}}_{Z_{tr}}^{-1}\mathbf{a}_{tr}(\theta)} \tag{30}$$

where  $\mathbf{a}_{tr}(\theta)$  in (30) can be defined as (31):

$$\mathbf{a}_{tr}(\theta) = \left[1, e^{j\frac{2\pi}{\lambda}d \sin \theta}, \dots, e^{j\frac{2\pi}{\lambda}(J-1)d \sin \theta}\right]^T \tag{31}$$

### 4.4. Spatial Smoothing Capon and ADVTR Capon Algorithm

The spatial smoothing technique is applied to the Capon algorithm and ADVTR Capon algorithm respectively. For the Capon algorithm:  $\hat{\mathbf{R}}_Y$  in (27) is replaced by  $\mathbf{R}_{YY}$  in (20) and  $\mathbf{a}(\theta)$  in (27) is replaced by the steering vector of each subarray (i.e., the dimensions of  $\mathbf{a}(\theta)$  are the same as those of the subarray) when spectral peak is being searched. So the spectrum function for spatial smoothing Capon algorithm can be obtained:

$$P_s(\theta) = \frac{1}{\mathbf{a}_s^H(\theta)\mathbf{R}_{YY}^{-1}\mathbf{a}_s(\theta)} \tag{32}$$

The DOA value of the target can be gained by searching the spectral peak of the Equation (32), in which  $\mathbf{a}_s(\theta)$  is the steering vector for spatial smoothing Capon algorithm expressed as (33):

$$\mathbf{a}_s(\theta) = \left[ 1, e^{-j\frac{2\pi}{\lambda}d \sin \theta}, \dots, e^{-j\frac{2\pi}{\lambda}(ns-1)d \sin \theta} \right]^T \quad (33)$$

For the ADVTR Capon algorithm,  $\hat{\mathbf{R}}_{Z_{tr}}$  and  $\mathbf{a}_{tr}(\theta)$  in (30) are replaced by  $\mathbf{R}_{ZZ}$  in (23) and the steering vector  $\mathbf{a}_{trs}(\theta)$  of each subarray when spectral peak is being searched. So the spectrum function for spatial smoothing ADVTR Capon algorithm can be obtained:

$$P_{trs}(\theta) = \frac{1}{\mathbf{a}_{trs}^H(\theta) \mathbf{R}_{ZZ}^{-1} \mathbf{a}_{trs}(\theta)} \quad (34)$$

The DOA value of the target can be gained by searching the spectral peak of the (34), in which  $\mathbf{a}_{trs}(\theta)$  is the steering vector for spatial smoothing ADVTR Capon algorithm expressed as (35):

$$\mathbf{a}_{trs}(\theta) = \left[ 1, e^{j\frac{2\pi}{\lambda}d \sin \theta}, \dots, e^{j\frac{2\pi}{\lambda}(ns-1)d \sin \theta} \right]^T \quad (35)$$

#### 4.5. Computational Complexity of Smoothing Capon and ADVTR Capon Algorithm

Assuming that the number of snapshot is  $L$ , the grid is divided into  $K$  angles when searching for spatial spectrum. Other parameters can be seen in Sections 3 and 4. We mainly consider the operations on matrix and vector, ignoring other operations. The computational complexities of the conventional Capon and ADVTR Capon algorithm are shown in Table 1.

From the previous discussions, since the additional processes are introduced in ADVTR Capon algorithm, like VTR, re-emitting virtually and re-receiving virtually (see Figure 2), its computational complexity is higher than the conventional Capon algorithm. Considering the performance improvement provided by the ADVTR Capon algorithm, its computational complexity is acceptable.

**Table 1.** Computational complexity analysis.

| Algorithm   | Computational Complexity  |
|-------------|---|
| Capon       | $O(ns^2 \times L) + O(ns^3) + K \cdot O(ns^2 + ns)$                       |
| ADVTR Capon | $J \cdot O\{J(M+L)\} + O(ns^2 \times L) + O(ns^3) + K \cdot O(ns^2 + ns)$ |

## 5. Simulation Results

In this section we confirm our theoretical model through simulations. The simulation environment is as follows: shallow water waveguide, uniform sound speed environment (the sound speed is 1.5 km/s), the bottom is to be modeled as an Acousto-Elastic halfspace, the density is 2 kg/m<sup>3</sup> and the case of single objective. The simulation model has been shown in Figure 3, where the number of TRM (SRA) is 9, the interelement spacing is 0.75 m, the element 1 is 75 m from the sea surface, the depth of bottom is 500 m, the source depth is 78 m and the range between PS and the target is 2 km. In order to verify the validity of the proposed algorithm, two angles such as 0° and −5° are selected randomly to perform the simulations apart. In other words, target is located in 78 m and 253 m respectively. The signal transmitted by PS is a 1 kHz continuous wave (CW) signal. The simulation environment is shown in Table 2.

Bellhop special acoustic field simulation toolbox under MATLAB simulation environment is used to simulate the ocean sound field environment. The multiple reflection path by sea surface or bottom are ignored because the energy attenuation is too large, and only the three paths illustrated in Figure 3 are considered, then the various parameters used for simulation are obtained, as shown in Tables 3 and 4.

**Table 2.** Simulation environment.

| Simulation Condition        | Parameter    |
|-----------------------------|--------------|
| Attenuation                 | 2 (dB/m) kHz |
| Number of targets           | 1            |
| Number of elements          | 9            |
| Interelement spacing        | 0.75 m       |
| The depth of element 1      | 75 m         |
| The depth of bottom         | 500 m        |
| The source depth            | 78 m         |
| Target depth ( $0^\circ$ )  | 78 m         |
| Target depth ( $-5^\circ$ ) | 253 m        |
| The range                   | 2 km         |
| Number of multipath         | 3            |

**Table 3.** Simulation parameters target at  $0^\circ$ .

| Simulation Parameter | Value  |
|----------------------|--|
| Direction of arrival | $\{4.458^\circ, 0^\circ, -22.884^\circ\}$                          |
| Amplitude            | $\{4.99 \times 10^{-4}, 5.0 \times 10^{-4}, 2.92 \times 10^{-4}\}$ |
| Delay of element 1   | $\{1.3372291, 1.3333348, 1.4479731\}$ s                            |

**Table 4.** Simulation parameters target at  $-5^\circ$ .

| Simulation Parameter | Value   |
|----------------------|---|
| Direction of arrival | $\{19.396^\circ, -4.998^\circ, -18.498^\circ\}$                     |
| Amplitude            | $\{4.93 \times 10^{-4}, 4.98 \times 10^{-4}, 4.74 \times 10^{-4}\}$ |
| Delay of element 1   | $\{1.351145, 1.3386036, 1.4065851\}$ s                              |

Through the simulation, we can discover that the amplitudes of the same paths from the target to each element (e.g., the amplitude from the target to each element via the top-reflection) are very closer. Then for convenience, the amplitude information between PS and the target expressed in the table is the corresponding direct-path, top-reflection-path and bottom-reflection-path successively.

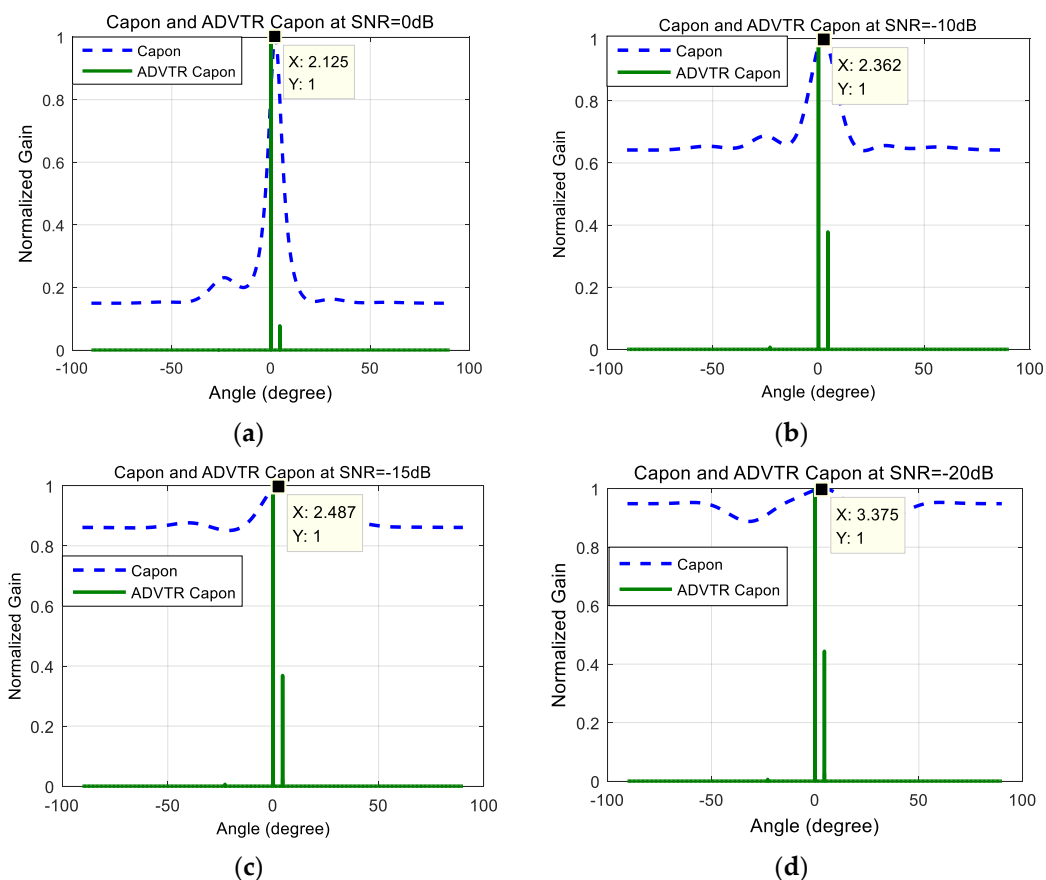
In order to compare the performance of the algorithm with or without ADVTR at the same conditions, SNR is defined as the ratio of signal to noise when the signal is received at the first time; while the noise doesn't added to the received signal on the second time on account of ADVTR.

Figure 5a–d shows the DOA estimation performance comparison with Capon estimator and ADVTR Capon estimator for target at  $0^\circ$  when the SNR is 0 dB,  $-10$  dB,  $-15$  dB, and  $-20$  dB; Figure 6a–d shows the DOA estimation performance comparison with Capon estimator and ADVTR Capon estimator for target at  $-5^\circ$  when the SNR is 0 dB,  $-10$  dB,  $-15$  dB and  $-20$  dB. It can be seen from Figures 5 and 6 that:

- (1) Relative to the Capon algorithm, the ADVTR Capon algorithm can estimate accurately the expected value of the target, whose energy of the main lobe is far higher than its corresponding sidelobes and resolution is higher whether the target is at  $0^\circ$  or  $-5^\circ$ . Taking a SNR of  $-10$  dB plotted in Figure 6b when target is at  $-5^\circ$  as an example, we can find that ADVTR Capon estimator has three peaks which correspond to the order of the multipath, whereas the conventional Capon estimator has only one peak and other two pieces of multipath information are lost. In addition, the ADVTR Capon estimator is more accurate with the highest peak in its spectrum observed at  $-5^\circ$ , much closer to the simulated DOA of  $4.998^\circ$  and with much finer resolution (smaller lobes). The conventional Capon DOA estimator has a value of  $-3.769^\circ$ .
- (2) The main reason for the result (1) is that relative to the conventional Capon algorithm, the operation of TR and re-transmitting to the channel in ADVTR is performed in the computer,

it will be focused virtually on the target according to the focusing characteristics of TR. The process is equivalent to the beamforming process used in the array signal processing, but TR method can focus the beam towards the DOA taking advantage of multipath and its adaptive focusing characteristic, thus the energy focusing on the target is greater than beamforming. Therefore, the DOA estimation angle is more accurate when ADVTR is introduced.

- (3) With the change of SNR from 0 dB to  $-20$  dB, the relations between main lobe and sidelobes for both the Capon and ADVTR Capon algorithms are the same that the energy of the sidelobes is higher and higher, and is getting closer to the main lobe. The difference is that the resolution for Capon algorithm is getting lower and lower, and the estimation deviation is more and more greater. However, the resolution for ADVTR Capon is almost not affected, and the target angle can be estimated without bias.
- (4) For the ADVTR method, the variation is mainly concentrated on the relation between the main lobe and sidelobes when SNR varies, and the main lobe energy can be accurately focused on the direct-path, so the estimated DOA values are almost unbiased. Because of above reasons the root mean square error (RMSE) is not analyzed. The main reason for this result is that the emphasis of this paper is the performance improvement of the Capon DOA estimation algorithm when the ADVTR method is introduced, rather than the channel estimation method, so the channel used in the focusing is the same as active detection one in the simulation and the channel estimation process is not carried out so that the effect of focusing is very ideal. If the channel estimation process is added before the virtual focusing is implemented in the virtual time reversal experiment, the focusing effect may go to the bad, and the result of the DOA estimation will be affected.



**Figure 5.** Capon estimator and ADVTR Capon estimator at  $\theta = 0^\circ$ . (a) SNR = 0 dB; (b) SNR =  $-10$  dB; (c) SNR =  $-15$  dB; (d) SNR =  $-20$  dB.

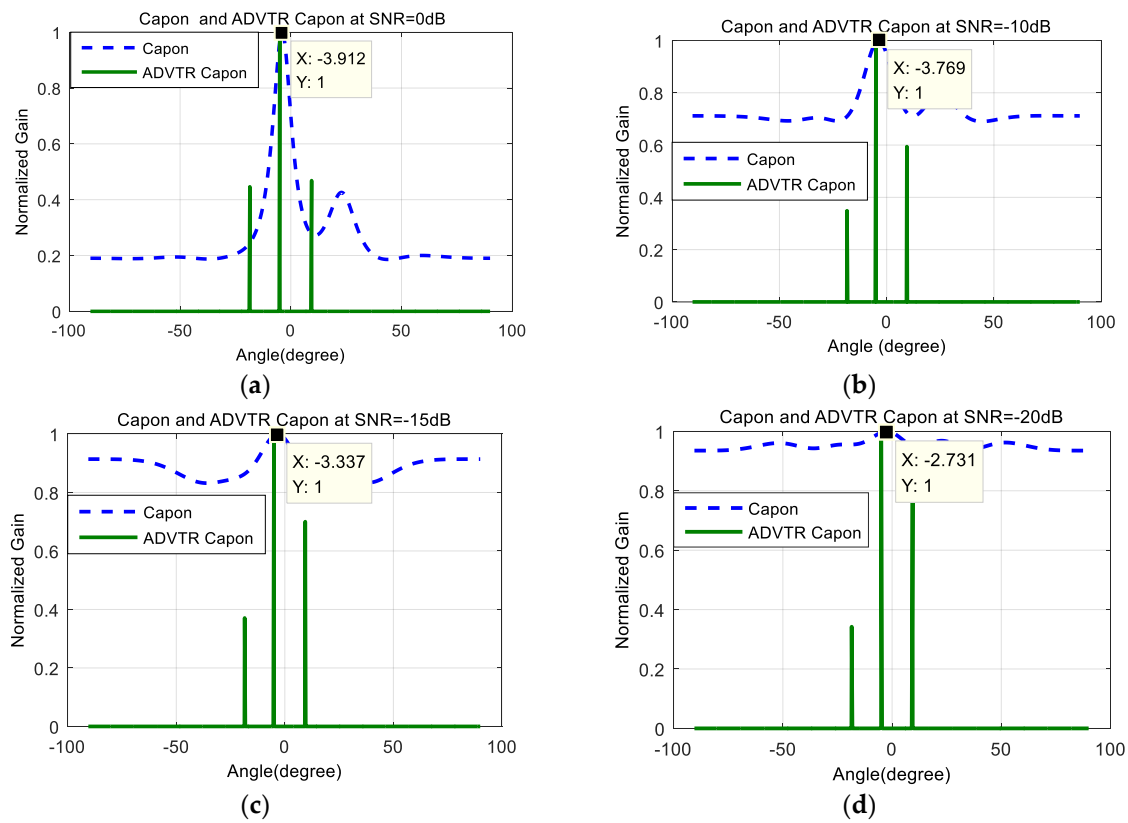


**Figure 6.** Capon estimator and ADVTR Capon estimator at  $\theta = -5^\circ$ . (a) SNR = 0 dB; (b) SNR = -10 dB; (c) SNR = -15 dB; (d) SNR = -20 dB.

## 6. Experiment Results

To further verify the effectiveness of the proposed algorithm, a real set of data deriving from the experiment conducted in the anechoic tank laboratory in 2015 is employed for DOA estimation in this section. The experiment setup is shown in Figure 7. Figure 8 shows the hydrophone array and underwater acoustic transducer (PS). Figure 9 is the transceiver and data acquisition field. All the sensors in our experiment are made from piezoelectric ceramics. The experiment diagrammatic sketch is shown in Figure 10.



**Figure 7.** The anechoic tank laboratory.



**Figure 8.** (a) The hydrophone array (b) The underwater acoustic transducer.



**Figure 9.** (a) The transceiver (b) The data acquisition field.

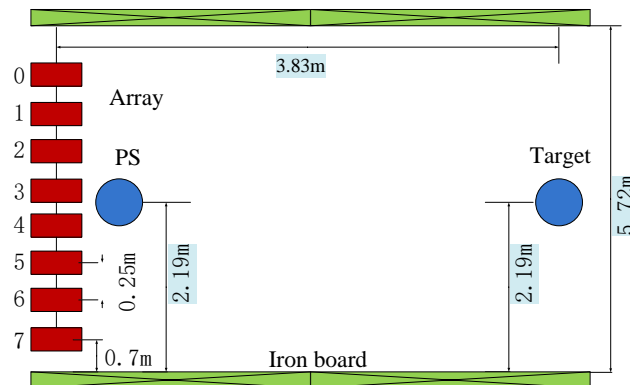


**Figure 10.** The data acquisition field.

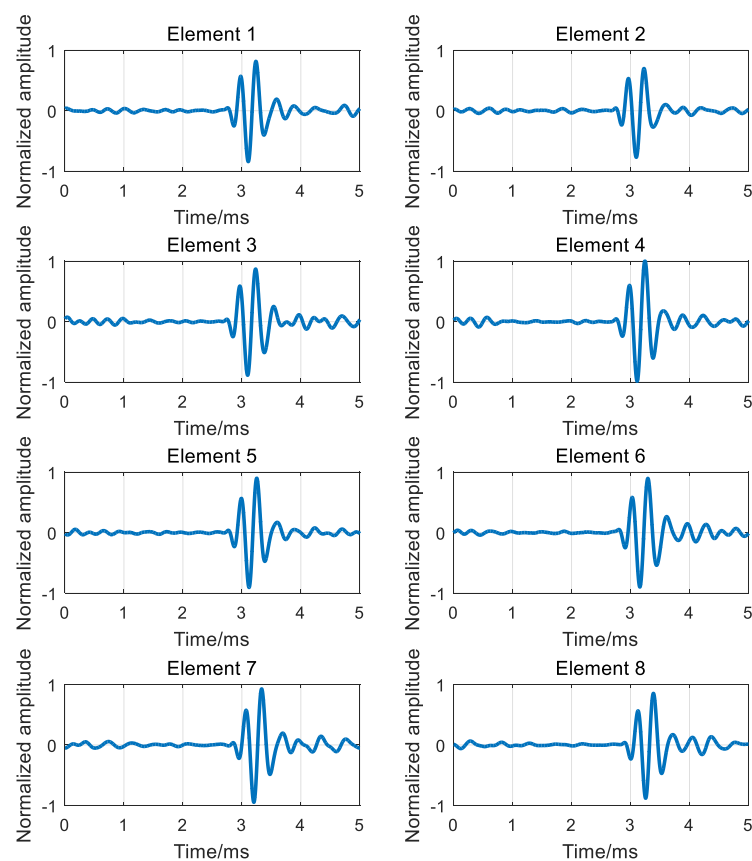
The test process is as follows: PS distributed in the center of the hydrophone array transmits a signal. In the real environment, the target is irradiated by the signal to produce the echo and then is received by the hydrophone array; while in the tank experiment, the transceiver is used to simulate the target echo: it will receive the transmitting signal from PS, scale it and return it into the tank to be received by the hydrophone array finally.

The whole device is placed horizontally in the tank and two pieces of iron sheet are adopted at the edge of the hydrophone array and transceiver to imitate the sea surface and floor respectively. The depth of both the array and transceiver is 0.8 m, and the range is 3.83 m. The PS and transceiver are aligned to the array center. The number of the array is 8, and the interelement spacing is 0.25 m. The PS transmitted a CW signal whose frequency is 3 kHz and width is one cycle. The overall experiment conditions are shown in Table 5.

**Table 5.** Experiment environment.

| Experiment Condition                               | Parameter |
|--|-----------|
| Distance between two pieces of iron                | 5.72 m    |
| Number of elements                                 | 8         |
| Interelement spacing                               | 0.25 m    |
| The position of elements 8 (from the bottom sheet) | 0.7 m     |
| Target position (from the bottom sheet)            | 2.19 m    |
| PS position (from the bottom sheet)                | 2.19 m    |
| Target depth                                       | 0.8 m     |
| Array depth  | 0.8 m     |
| The range  | 3.83 m    |
| DOA  | 0°        |
| PS frequency                                       | 3 KHz     |
| Sampling frequency                                 | 1.04 MHz  |

The first received signals of each element are shown in Figure 11. It can be seen from Figure 11 that the due to the multipath effects of the channel, transmitting signal of one cycle has different degrees of delay expansion at each receiving element through the channel, and the receiving signals of each element in Figure 11 can be understood as the superposition of the signals corresponding to multiple paths.

**Figure 11.** The first received signals of element 1–8.

By calculating the correlation between the received signal shown in Figure 11 and PS, the channel response functions between the target and each element can be obtained, as illustrated in Figure 12, which only takes the element 2 as an example and the other elements are similar to it. According to the ray model, each line in Figure 12 represents a path; meanwhile the horizontal axis and the vertical axis

represent the time and amplitude of the path respectively. As can be seen from Figure 12, there are 5 paths between the target and the element 2.

According to the process of ADVTR, the first received signals of each element will be time reversed and then re-emitted virtually to the estimated channel; then the TR signals received secondly by each element can be obtained by convoluting the TR signals of Figure 11 and the estimated channel response functions illustrated in Figure 12 as shown in Figure 13.

By comparing the received signals before and after TR as shown in Figures 11 and 13, it can be obtained that the received signals after TR are focused in time and the delay difference caused by multipath is overcome to a certain extent.

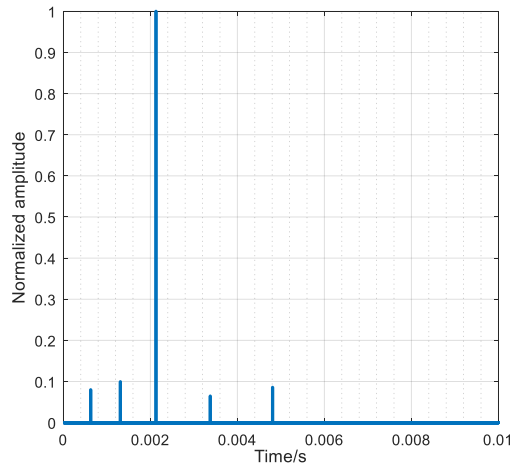


Figure 12. The estimated channel transfer functions between the target and element 2.

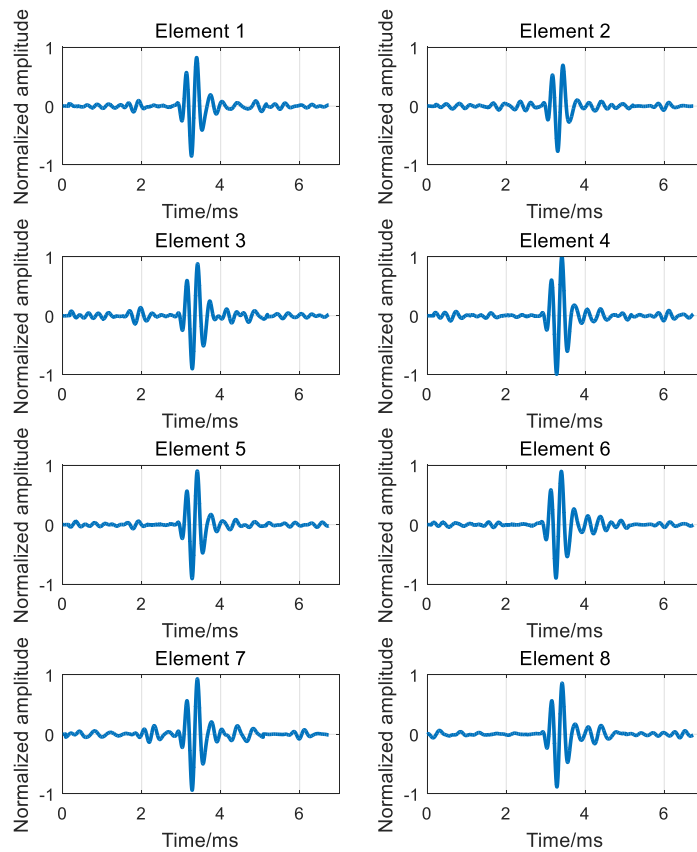
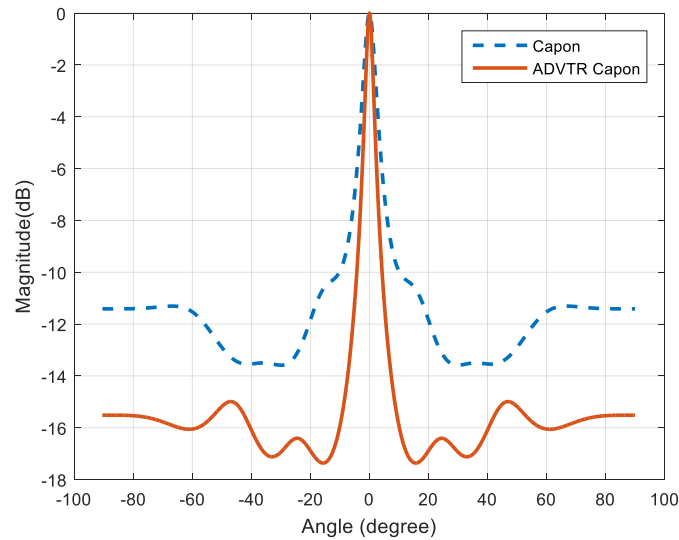


Figure 13. The second received signals of element 1–8.

For the signals shown in Figures 11 and 13, the covariance matrices re-calculated individually and the algorithms proposed in Section 4 are employed to estimate the DOA of the target. The estimation results are shown in Figure 14.



**Figure 14.** Capon estimator and ADVTR Capon estimator in the tank.

It can be seen from Figure 14 that both the two methods can estimate the target accurately, whose estimated values are  $-0.0020^\circ$ . The reason for this result is that the experimental environment in the tank can be considered as a noiseless one, so there are basically no differences between the two methods. It's only that the ADVTR method has a relatively lower sidelobes and higher resolution. This result verifies the effectiveness of ADVTR method to some extent.

Next we will discuss the difference between the two methods under the noise environment which is much closer to the real situation. Therefore the Gauss white noise is artificially added to the first received signal. Then the above processes such as channel estimation, time reversal, the signals received secondly, the calculation of covariance matrix and DOA estimation are repeated. The performance comparison of both methods can be obtained as illustrated in Figure 15 when the SNR is  $-8$  dB.

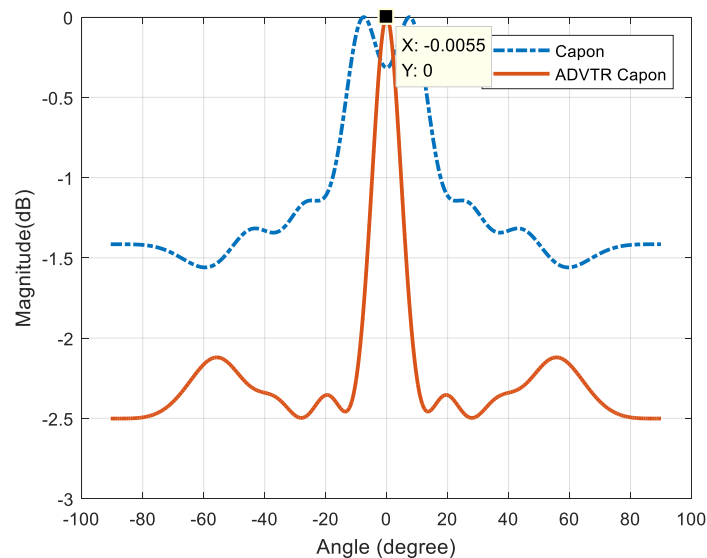


**Figure 15.** Capon estimator and ADVTR Capon estimator in the tank when SNR is  $-8$  dB.

We can see from Figure 15 that when SNR is  $-8$  dB the Capon estimator can't estimate the angle of the target where two false peaks appear while the ADVTR Capon one is more accurate with the highest peak in its spectrum observed at  $-0.0055^\circ$  which is much closer to the true value of  $0^\circ$  and with much finer resolution (smaller lobes).

Due to the randomness of noise, the estimation results of Figure 15 are not enough to illustrate the problem. Thus Monte Carlo simulation tests are introduced. Environmental noise with different intensity is added, and Monte Carlo simulation based on 1000 runs for each SNR with and without TR is performed, as shown in Figure 16.

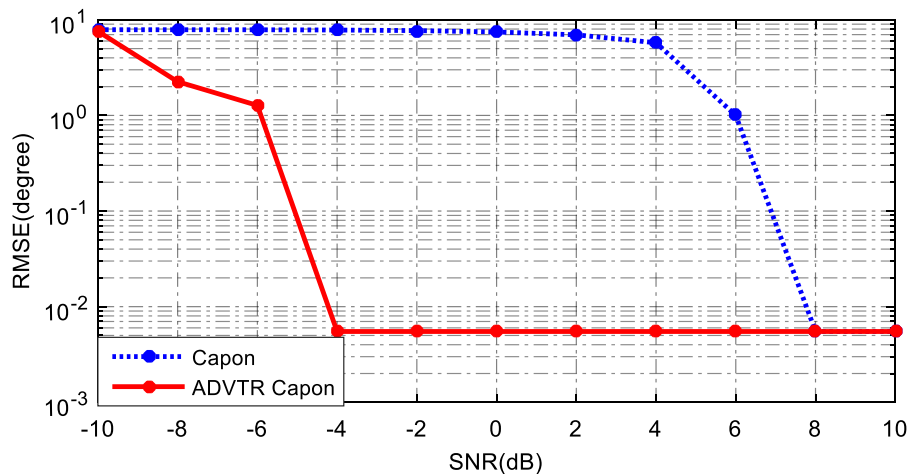


**Figure 16.** RMSE for Capon estimator and ADVTR Capon estimator in the tank.

As can be seen from Figure 16 that RMSE estimated by the ADVTR Capon algorithm is smaller than the conventional Capon algorithm, especially when the SNR is very low, the advantage of ADVTR Capon algorithm is particularly obvious. Figure 16 illustrates the good performance of the ADVTR DOA estimation model on low SNR.

## 7. Conclusions and Future Work

In this paper, we use the ADVTR method to study the performance of underwater target DOA in the presence of multipath, and a DOA estimation algorithm based on the ADVTR Capon algorithm is proposed. Firstly, based on the ray theory, a conventional multipath DOA estimation model and an ADVTR DOA estimation model for ULA are established, and then the model is estimated with the spatial smoothing Capon algorithm. The simulation results show that the DOA estimator including ADVTR, compared with the conventional method without TR, has a more accurately estimated value, a higher resolution and a stronger ability to suppress sidelobes, so that the target DOA estimation can be achieved in the case of low SNR and multipath. The tank experiment further verifies the effectiveness of the proposed method.

As part of the future work, we intend to extend the proposed approaches to the following points in the future:

- (1) The DOA estimation in this paper is concentrated upon a single target, so the multi-objective estimation on TR will be carried out in the future research.
- (2) The location of underwater target can be achieved combining range estimator on TR with DOA estimator in this paper, and the lake experimental research will be carried out in the future.
- (3) The deduction in the paper is based on the narrow band signal, and the DOA estimation of broadband signal is the future research work.
- (4) The Capon algorithm is applied for DOA estimation in this paper, and other popular algorithms such as MUSIC will be studied in the future work.

**Author Contributions:** Conceptualization, H.J., H.W., Z.L. and X.S.; Data curation, X.S.; Formal analysis, H.J.; Funding acquisition, H.W. and X.S.; Methodology, H.J., H.W., Z.L. and X.S.; Project administration, H.W. and X.S.; Resources, H.W. and X.S.; Software, H.J.; Supervision, H.W. and X.S.; Writing—original draft, H.J.; Writing—review & editing, H.J., H.W., Z.L. and X.S.

**Funding:** This research was supported by the National Key R&D Program of China (Grant No. 2016YFC1400200) and the National Natural Science Foundation of China (Grant No. 61571365, 61571367, 61401364 and 61671386).

**Acknowledgments:** The acquisition of tank experimental data came from the hard work of Fuzhou Yang and Zhichen Zhang. Tianyi Jia provided many helps on the algorithm design and Matlab simulation experiments. Zhichen Zhang gave lots of helps for writing the manuscript. We will express our sincere thanks to them for their help.

**Conflicts of Interest:** The authors declare no conflict of interest.

## References

1. Van Trees, H.L. *Optimal Array Processing Theory. Part IV of Detection, Estimation, and Modulation Theory*; John Wiley & Sons, Inc.: New York, NY, USA, 2002.
2. Wang, B.; Wang, W.; Gu, Y.I.; Lei, S.J. Underdetermined DOA Estimation of Quasi-Stationary Signals Using a Partly-Calibrated Array. *Sensors* **2017**, *17*, 702. [[CrossRef](#)] [[PubMed](#)]
3. Donoho, D.L. Compressed sensing. *IEEE Trans. Inform. Theory* **2006**, *52*, 1289–1306. [[CrossRef](#)]
4. Tsaig, Y.; Donoho, D.L. Extensions of compressed sensing. *Signal Process.* **2006**, *86*, 549–571. [[CrossRef](#)]
5. Fortunati, S.; Grasso, R.; Gini, F.; Greco, M.S.; Lepage, K. Single-snapshot DOA estimation by using Compressed Sensing. *EURASIP J. Adv. Signal Process.* **2014**, *2014*, 120. [[CrossRef](#)]
6. Kang, C.Y.; Li, Q.Y.; Jiao, Y.M.; Li, J.; Zhang, X.H. Direction of arrival estimation and signal recovery for underwater target based on compressed sensing. In Proceedings of the 8th International Congress on Image and Signal Processing (CISP 2015), Shenyang, China, 14–16 October 2015; pp. 1277–1282.
7. Guo, M.R.; Tao, C.; Ben, W. An Improved DOA Estimation Approach Using Coarray Interpolation and Matrix Denoising. *Sensors* **2017**, *17*, 1140. [[CrossRef](#)] [[PubMed](#)]
8. Li, W.X.; Zhang, Y.; Lin, J.Z.; Guo, R.; Chen, Z.P. Wideband Direction of Arrival Estimation in the Presence of Unknown Mutual Coupling. *Sensors* **2017**, *17*, 230. [[CrossRef](#)] [[PubMed](#)]
9. Daeipour, E.; Blair, W.D.; Bar-Shalom, Y. Bias Compensation and Tracking with Monopulse Radars in the Presence of Multipath. *IEEE Trans. Aerosp. Electron. Syst.* **1997**, *33*, 863–882. [[CrossRef](#)]
10. Zhang, R.N.; Wang, S.C.; Lu, X.F.; Duan, W.M.; Cai, L. Two-dimensional DOA estimation for multipath propagation characterization using the array response of PN-sequences. *IEEE Trans. Wirel. Commun.* **2016**, *15*, 341–356. [[CrossRef](#)]
11. Fink, M. Time reversal of ultrasonic fields. Part I: Basic principles. *IEEE Trans. Ultrason. Ferroelectron. Freq. Contr.* **1992**, *39*, 555–566. [[CrossRef](#)] [[PubMed](#)]
12. Moura, J.M.F.; Jin, Y.W. Detection by time reversal: Single antenna. *IEEE Trans. Signal Process.* **2007**, *55*, 187–201. [[CrossRef](#)]
13. Fink, M. Time reversed acoustics. *Phys. Today* **1997**, *50*, 34–40. [[CrossRef](#)]
14. Fink, M. Time-reversed acoustics. *Sci. Am.* **1999**, 91–97. [[CrossRef](#)]
15. Fink, M.; Prada, C. Acoustics time-reversed mirrors. *Inverse Probl.* **2001**, *17*, R1–R38. [[CrossRef](#)]
16. Fink, M.; Prada, C.; Wu, F.; Cassereau, D. Self focusing in inhomogeneous media with time reversal acoustic mirrors. In Proceedings of the IEEE Ultrasonics Symposium, Montreal, QC, Canada, 3–6 October 1989; pp. 681–686.
17. Prada, C.; Wu, F.; Fink, M. The iterative time reversal mirror: A solution to self-focusing in the pulse echo mode. *J. Acoust. Soc. Am.* **1991**, *90*, 1119–1129. [[CrossRef](#)]
18. Kuperman, W.A.; Hodgkiss, W.S.; Song, H.C. Phase conjugation in the ocean: Experimental demonstration of an acoustic time-reversal mirror. *J. Acoust. Soc. Am.* **1998**, *103*, 25–40. [[CrossRef](#)]
19. Khosla, S.R.; Dowling, D.R. Time-reversing array retrofocusing in simple dynamic underwater environments. *J. Acoust. Soc. Am.* **1998**, *104*, 3339–3350. [[CrossRef](#)]
20. Song, H.C.; Kuperman, W.A.; Hodgkiss, W.S. Iterative time reversal in the ocean. *J. Acoust. Soc. Am.* **1999**, *105*, 3176–3184. [[CrossRef](#)]
21. Lerosey, G.; Rosny, J.D.; Tourin, A.; Derode, A.; Montaldo, G.; Fink, M. Time reversal of electromagnetic waves. *Phys. Rev. Lett.* **2004**, *92*, 194301. [[CrossRef](#)] [[PubMed](#)]

22. Henty, B.E.; Stancil, D.D. Multipath enabled super-resolution for RF/microwave communication using phase-conjugate arrays. *Phys. Rev. Lett.* **2004**, *93*, 243904. [[CrossRef](#)] [[PubMed](#)]
23. Devaney, A.J.; Marengo, E.A.; Gruber, F.K. Time-reversal-based imaging and inverse scattering of multiply scattering point targets. *J. Acoust. Soc. Am.* **2005**, *118*, 3129–3138. [[CrossRef](#)]
24. Sabra, K.G.; Roux, P.; Song, H.C.; Hodgkiss, W.S.; Kuperman, W.A. Experimental demonstration of iterative time-reversed reverberation focusing in a rough waveguide: Application to target detection. *J. Acoust. Soc. Am.* **2006**, *120*, 1305–1314. [[CrossRef](#)]
25. Li, C.X.; Xu, W.; Li, J.L.; Gong, X.Y. Time-Reversal Detection of Multidimensional Signals in Underwater Acoustics. *IEEE J. Ocean. Eng.* **2011**, *36*, 61–71. [[CrossRef](#)]
26. Jin, Y.W.; Moura, J.M.F. Time-Reversal Detection Using Antenna Arrays. *IEEE Trans. Signal Process.* **2009**, *57*, 1396–1414.
27. Sheng, X.L.; Bao, X.Z.; Hui, J.Y.; Liang, G.L. Underwater passive location technology using dummy time-reversal mirror. In Proceedings of the 3rd International Conference on Image and Signal Processing (ICISP 2008), Cherbourg-Octeville, France, 1–3 July 2008; pp. 605–612.
28. Yu, Z.B.; Zhao, H.F.; Gong, X.Y.; Chapman, N.R. Time-Reversal Mirror-Virtual Source Array Method for Acoustic Imaging of Proud and Buried Targets. *IEEE J. Ocean. Eng.* **2016**, *41*, 382–394.
29. Edelmann, G.; Akal, T.; Hodgkiss, W.S.; Kim, S.; Kuperman, W.A.; Song, H.C. An initial demonstration underwater acoustic communication using time reversal. *IEEE J. Ocean. Eng.* **2002**, *27*, 602–609. [[CrossRef](#)]
30. Wang, B.B.; Wu, Y.L.; Han, F.; Yang, Y.-H.; Liu, K.J.R. Green Wireless Communications: A Time-Reversal Paradigm. *IEEE J. Select. Areas Commun.* **2011**, *29*, 1698–1710. [[CrossRef](#)]
31. Song, H.C. An Overview of Underwater Time-Reversal Communication. *IEEE J. Ocean. Eng.* **2016**, *41*, 644–655. [[CrossRef](#)]
32. Foroozan, F.; Asif, A. Cramer-Rao Lower Bound for Time Reversal Active Array Direction of Arrival Estimation in Multipath Environment. In Proceedings of the 2010 IEEE ICASSP, Dallas, TX, USA, 14–19 March 2010; pp. 2646–2649.
33. Abadi, S.H.; Song, H.C.; Dowling, D.R. Broadband sparse-array blind deconvolution using frequency-difference beamforming. *J. Acoust. Soc. Am.* **2012**, *132*, 3018–3029. [[CrossRef](#)] [[PubMed](#)]
34. Foroozan, F.; Asif, A. Time Reversal Direction of Arrival Estimation with Cramer-Rao Bound Analysis. In Proceedings of the IEEE Globecom 2010, Miami, FL, USA, 6–10 December 2010; pp. 1–5.
35. Foroozan, F.; Asif, A. Time Reversal Based Active Array Source localization. *IEEE Trans. Signal Process.* **2011**, *59*, 2655–2668. [[CrossRef](#)]
36. Foroozan, F.; Asif, A. Direction Finding Algorithms for time reversal MIMO radars. In Proceedings of the 2011 IEEE SSP, Nice, France, 28–30 June 2011; pp. 433–436.
37. Foroozan, F.; Asif, A. Time Reversal MIMO Radar for Angle-Doppler Estimation. In Proceedings of the 2012 IEEE SSP, Ann Arbor, MI, USA, 5–8 August 2012; pp. 860–863.
38. Foroozan, F.; Asif, A.; Jin, Y.W. Cramer-Rao bounds for time reversal MIMO radars with multipath. *IEEE Trans. Aerosp. Electron. Syst.* **2016**, *52*, 137–154. [[CrossRef](#)]
39. Sajjadih, M.H.S.; Asif, A. Compressive Sensing Time Reversal MIMO Radar: Direction and Doppler Frequency Estimation. *IEEE Signal Process. Lett.* **2015**, *22*, 1283–1287. [[CrossRef](#)]
40. Fu, Y.Q.; Liu, W.; Bai, R.J.; Li, J.; Wang, J. A Novel Virtual Time Reversal Method for Passive Direction of Arrival Estimation. *Math. Probl. Eng.* **2015**, *2015*, 1–12. [[CrossRef](#)]
41. Ciunzo, D.; Romano, G.; Solimene, R. Performance Analysis of Time-Reversal MUSIC. *IEEE Trans. Signal Process.* **2015**, *63*, 2650–2662. [[CrossRef](#)]
42. Ciunzo, D.; Rossi, P.S. Noncolocated Time-Reversal MUSIC: High-SNR Distribution of Null Spectrum. *IEEE Signal Process. Lett.* **2017**, *24*, 397–401. [[CrossRef](#)]
43. Ciunzo, D.; Rossi, P.S. On the asymptotic distribution of time-reversal MUSIC null spectrum. *Dig. Signal Process.* **2017**, *69*, 50–58. [[CrossRef](#)]
44. Borcea, L.; Papanicolaou, G.; Tsogka, C.; Berryman, J. Imaging and time reversal in random media. *Inverse Probl.* **2002**, *18*, 1247–1279. [[CrossRef](#)]
45. Shi, G.; Nehorai, A. Maximum likelihood estimation of point scatterers for computational time-reversal imaging. *Commun. Inf. Syst.* **2005**, *5*, 227–256.
46. Zeng, X.L.; Yang, M.L.; Chen, B.X.; Jin, Y.W. Low Angle Direction of Arrival Estimation by Time Reversal. In Proceedings of the 2017 IEEE ICASSP, New Orleans, LA, USA, 5–9 March 2017; pp. 3161–3165.

47. Silva, A.; Jesus, S.; Gomes, J.; Barroso, V. Underwater acoustic communication using a virtual electronic time-reversal mirror approach. In Proceedings of the 5th European Conference on Underwater Acoustics, Lyon, France, 10–13 July 2000; Volume V.
48. Yang, F.Z.; Wang, H.Y.; Shen, X.H.; Jing, H.X. Super-direction element distribution model of NLA based on TR. *J. Shanghai Jiao Tong Univ.* **2013**, *47*, 1907–1910.
49. Shao, J.F.; Zhang, X.M.; Liu, Y.H.; Yang, F.Z. Estimation of Time Reversal Target DOA over Underwater Acoustic Multipath Time-varying Channel. In Proceedings of the 2014 IEEE China SIP, Xi'an, China, 9–13 July 2014; pp. 795–799.
50. Yang, F.Z.; Wang, H.Y.; Shen, X.H.; Hua, F. The performance of time reversal beam-forming by linear array. In Proceedings of the 2012 IEEE China SIP, Hong Kong, China, 12–15 August 2012; pp. 650–653.
51. Zhang, Z.C.; Wang, H.Y.; Liu, Z.G.; Shen, X.; Jiang, Z. A new LFM detection algorithm based on AVTR-FrFT for active sonar system. In Proceedings of the 2017 IEEE China SIP, Xiamen, China, 22–25 October 2017; pp. 1–5.
52. Dowling, D.R. Acoustic pulse compression using passive phase-conjugate processing. *J. Acoust. Soc. Am.* **1994**, *95*, 1450–1458. [[CrossRef](#)]
53. Zhang, Z.C.; Jiang, Z.; Wang, H.Y.; Liu, Z.G.; Jing, H.X. Combination of time-reversal focusing and Fractional Fourier Transform for detection of underwater target in multipath environments. In Proceedings of the 2017 OCEANS—Anchorage, Anchorage, AK, USA, 18–21 September 2017; pp. 1–5.
54. Gu, J.J.; Wang, H.Y. Influence of underwater acoustic multipath structure on time reversal passive detection. In Proceedings of the 2012 IEEE China SIP, Hong Kong, China, 12–15 Augst 2012; pp. 779–782.
55. Jia, T.Y.; Wang, H.Y.; Shen, X.H.; Liu, X.C. Direction of Arrival Estimation with Co-prime Arrays via Compressed Sensing Methods. In Proceedings of the Oceans 2016—Shanghai, Shanghai, China, 10–13 April 2016; pp. 1–5.



© 2018 by the authors. Licensee MDPI, Basel, Switzerland. This article is an open access article distributed under the terms and conditions of the Creative Commons Attribution (CC BY) license (<http://creativecommons.org/licenses/by/4.0/>).